Desalination and Water Treatment
www.deswater.com

doi: 10.5004/dwt.2021.27727

237 (2021) 64–76
October

Study on sodium functionalized ultrasonic-diatomite and its performance for phosphorus removal

Gufeng Li, Min Yang, Xuemei Ding, Wei Tan, Guizhen Li, Shuju Fang, Hongbin Wang*

School of Chemistry and Environment, Yunnan Minzu University, Kunming 650500, Yunnan, China,
emails: wanghb2152@126.com (H.B. Wang), 1250191263@qq.com (G.F. Li), 826677468@qq.com (M. Yang),
1242350943@qq.com (X.M. Ding), 317366182@qq.com (W. Tan), 325865775@qq.com, (G.Z. Li), 743372267@qq.com (S.J. Fang)

Received 6 April 2021; Accepted 12 August 2021

ABSTRACT

The sodium functionalized ultrasonic-diatomite (U-D-Na) was used as an adsorbent to remove phosphorus from an aqueous solution. After simple ultrasonic purification, diatomite was functionalized by the cheap NaCl reagent to prepare U-D-Na. The microstructure and properties of U-D-Na were achieved by scanning electron microscopy, energy-dispersive X-ray spectroscopy, X-ray diffraction, Brunauer–Emmett–Teller, Fourier-transform infrared spectroscopy and thermogravimetry/differential scanning calorimetry. The effect on the contact time, the temperature, the dosage of adsorbent, pH and the initial concentration of phosphorus were investigated during the adsorption kinetics and equilibrium studies. The U-D-Na exhibited that the adsorption efficiency reached more than 90% at optimal conditions. Multiple cycles of adsorption and desorption tests showed that the adsorbent performed good renewability. The experimental values were coincidence with the pseudo-second-order kinetic model and the Langmuir isotherm model. Also, thermodynamic parameters such as the $\Delta G°$, $\Delta H°$ and $\Delta S°$ illustrated that the adsorption process is essentially exothermic and spontaneous. The results indicated that a promising application prospect for water pollution management by U-D-Na.

Keywords: Diatomite; Ultrasonic; Sodium; Adsorption; Phosphorus

1. Introduction

Excessive phosphorus content will lead to severe water eutrophication, which threatens the ecosystems and human health [1]. The water environment is considered eutrophication when phosphorus concentration in the water body exceeds 0.02 mg/L by EPA criterion [2]. Conventional technology for phosphorus removal includes biological methods, chemical precipitation and adsorption [3–6]. Compared with other technologies, the adsorption method has the advantages of economy, stability, simple process, high efficiency, environmental protection and strong regeneration ability [7,8]. It is currently a more popular phosphorus removal method. Adsorbent materials with good absorptive effect because of their multi-pores structure and high specific surface area are widely applied to various water environments. At present, common adsorbent materials include diatomite, activated carbon, swell soil, zeolite, etc [9–13].

Diatomite is a widespread, cheap and stable adsorbent with excellent application prospects. It is formed after the remains of diatoms are deposited. The main component of diatomite is SiO_2 and contains a small amount of Al_2O_3, Fe_2O_3 and organic matter. Diatomite is characterized by

* Corresponding author.

porous structure and a huge specific surface area. Its surface is rich in hydroxyl groups, hydrogen bonds and silicon hydroxyl groups, and is generally chain-layered [14–16]. However, covered with impurities in the surface and pores, the adsorption efficiency of most raw diatomite is poor [17]. Therefore, it is of vital necessity to optimize the significant adsorption performance of diatomite by purifying and modifying. The modified diatomite loaded with lanthanum was prepared by Wang et al. [18], its maximum adsorption capacity for phosphorus is 80.90 mg/g. Lyngsie et al. [19] reported the novel absorbent that showed a remarkable absorption rate on phosphorus, the absorbent was modified by covering the calcined diatomite with iron oxide. It was found by Fan et al. [20] that zirconium modified diatomite has a significant effect of reducing the phosphorus content of the eutrophic lake. In short, the dephosphorization performance of diatomite is dramatically improved after modification. However, lanthanum, zirconium and other elements are relatively expensive, elements such as lanthanum take the potential risk of leakage [21]. Therefore, those elements are difficult to use in actual production. It is necessary to find an inexpensive but fine purification and modification method to expand the practical application of the diatomite in the treatment of phosphorus wastewater.

The main purification method of the raw diatomite includes chemical purification (acid leaching and alkaline leaching), physical purification (scrubbing and roasting) and physicochemical joint purification method (microwave-acid leaching method and ultrasonic-acid leaching method) [22]. Researches have shown that impurities of diatomite were destroyed via the cavitation effect in the ultrasound process [23]. Fine-grained clay impurities were shed from the surface, and at the same time, the structure was not destroyed by ultrasonic. These factors played a significant role in the porousness of diatomite. The active group of diatomite can adsorb phosphate by electrostatic attraction and ion exchange, but its activity and adsorption capacity are limited [24]; therefore, the metal salt is used as a modifier to enhance electrostatic attraction or ion exchange effect by loading metal cation on the diatomite, which supplies countless adsorption activity centers [25–28]. If NaCl is used as a modifying agent, the active group of diatomite may be activated by adding a certain amount of Na^+. Sodium-modified diatomite has excellent adsorption performance for anions such as phosphate by cation exchange and electrostatic attraction.

The main objective of this work attempts to remove phosphorus faster and more efficiently from wastewater with U-D-Na. Physical characteristics of U-D-Na were determined by scanning electron microscopy (SEM), energy-dispersive X-ray spectroscopy (EDS), X-ray diffraction (XRD), Brunauer–Emmett–Teller (BET), Fourier-transform infrared spectroscopy (FT-IR) and thermogravimetry/differential scanning calorimetry (TG/DSC). The optimal experiment conditions for phosphorus removal by U-D-Na were determined. Furthermore, the adsorption mechanism was discussed based on the isotherm, kinetic and thermodynamic models. This study may lay the foundation and provide a candidate adsorbent for the mitigation of eutrophication through the discussion of the adsorption mechanism.

2. Materials and methods

2.1. Materials

The raw diatomite was collected from Xundian, Yunnan, China. Sodium chloride (NaCl, GR) was purchased from Xilong Scientific Co., Ltd., China; monopotassium phosphate (KH_2PO_4, GR) was bought from Tianjin Guangfu Fine Chemical Research Institute, China. Sodium hydroxide (NaOH), sulfuric acid (H_2SO_4) and sodium carbonate (Na_2CO_3) were of analytical grade and were prepared by distilled water or secondary deionized water in the experiments.

2.2. Preparation and characterization of U-D-Na

2.2.1. Preparation

The raw diatomite was mixed with distilled water in the beaker. Six raw diatomite samples with the same weights were purified by a 150 w ultrasonic cleaner for 1 h; the solid was separated and washed to neutral pH with distilled water, and then dried in vacuum at 110°C to obtain the purified diatomite samples. 5 g of six purified diatomite samples were put into conical flasks and then added 250 mL NaCl solutions with six different mass fractions (0.50%, 1.00%, 3.00%, 5.00%, 7.00% and 9.00%) to it respectively, the mixtures were stirred for 2 h at 95°C. The samples were rinsed with distilled water until neutral pH and no Cl^- presented, and then dried in vacuum at 110°C. Subsequently, the samples were placed into a muffle furnace for calcination under an atmosphere at 400°C for 2 h. The U-D-Na was put into desiccator and stored for later use.

2.2.2. Characterization

The surface morphology of diatomite treated in different ways was studied by SEM (Nova NanoSEM 450, FEI, America). The element content of different diatomite was characterized by EDS (D/Max-3B, Rigaku Corporation, Japan). XRD (2SX100e, Rigaku Corporation, Japan) and FT-IR (Nicolet iS10, America) have detected the composition and functional groups of different diatomite. The surface area, pore size, and pore volume were all determined using the BET (ASAP 2460 Version 3.01, Micromeritics, America). TG/DSC (STA449F3, NETZSCH-Gerätebau GmbH, Germany) was used to analyze the weight change rate of diatomite treated with different treatments.

2.3. Adsorption studies

2.3.1. Batch adsorption experiment

Groups of adsorption experiments were performed in 100 mL conical flasks in which 50 mL simulated wastewater containing phosphate and adsorbent, and then the conical flasks were placed into a constant temperature oscillator. The effects of the different contact temperature (15°C–45°C), the different contact time (5–80 min), the different weight of U-D-Na (0.40–2.00 g), the pH value range (2–14) and the initial phosphate concentration (5–35 mg/L) were testified on the removal efficiency of phosphate to ensure the adsorption performance of U-D-Na. After separation of centrifuged (1500 rpm for

20 min), 10 mL of supernatant was diluted with deionized water, and the final phosphate concentrations in it were detected by molybdenum-antimony anti-spectrophotometry. The removal efficiency was calculated from the following equations:

$$q = \frac{(C_0 - C_e) \times V}{m} \quad (1)$$

$$R = \frac{C_0 - C_e}{C_0} \times 100\% \quad (2)$$

where C_0 (mg/L) is the initial concentration of phosphate, C_e (mg/L) is the equilibrium concentration of phosphorus, m is the mass of the adsorbent (g), and V is the volume of the simulated wastewater (L).

2.3.2. Regenerate experiment

After adsorption phosphate, the above sediment was desorbed by the different regenerant with a mass fraction of 5.00% (HCl, Na_2CO_3, NaOH, and NaCl) and distilled water, respectively under optimized desorption conditions. After separation of centrifuging, the final phosphate concentrations in it were analyzed after dilution. After adsorption-regeneration cycles were repeated five times at 50°C, the adsorption property was compared.

3. Results and discussion

3.1. Study on preparation of functional diatomite

3.1.1. Optimization of preparation conditions

Table 1 reveals that the purification effect of two methods including wash and ultrasound on diatomite used as the phosphate adsorbent. Compared with raw diatomite (D), the removal efficiency of ultrasonic diatomite (U-D) increased from 14.65% to 50.08%. The phosphate removal efficiency of U-D was superior to that of D and washed diatomite (W-D). One reason why the adsorption efficiency of U-D was higher is that the cavitation effect of ultrasonic can dredge blocked pores and improve pore size distribution. The adsorption trend of U-D functionalized by La_2O_3, NaCl and $LaCl_3$ respectively can be seen in Table 2. The effects of three modified diatomite are quite remarkable, and the removal efficiencies can reach more than 94%. NaCl reagent has the double advantages of being both facile and cheap, therefore it was selected as the modifier. The phosphate removal performance of U-D-Na functionalized by NaCl reagent with different mass fractions was illustrated in Fig. 1A. The trend of removal efficiency rose to a high point when the mass fraction of NaCl reagent employed was 5.00%. As a result, the optimal mass fraction of the modifier in the preparation was 5.00%. With the increase of the mass fraction of NaCl, more and more sites on the surface of diatomite may be continuously occupied by Na. The efficiency for removing phosphate reached its

Table 1
Removal efficiency of D, W-D and U-D

Adsorbent	Dosage of adsorbent (g)	Removal efficiency (%)
D	0.80	14.65
W-D	0.80	32.32
U-D	0.80	50.08

Table 2
Effect of different modifier on the removal efficiency

Modifier	Dosage of adsorbent (g)	Mass fraction of the modifier (%)	Removal efficiency (%)
La_2O_3	0.80	5.00	94.75
NaCl	0.80	5.00	97.44
$LaCl_3$	0.80	5.00	99.29

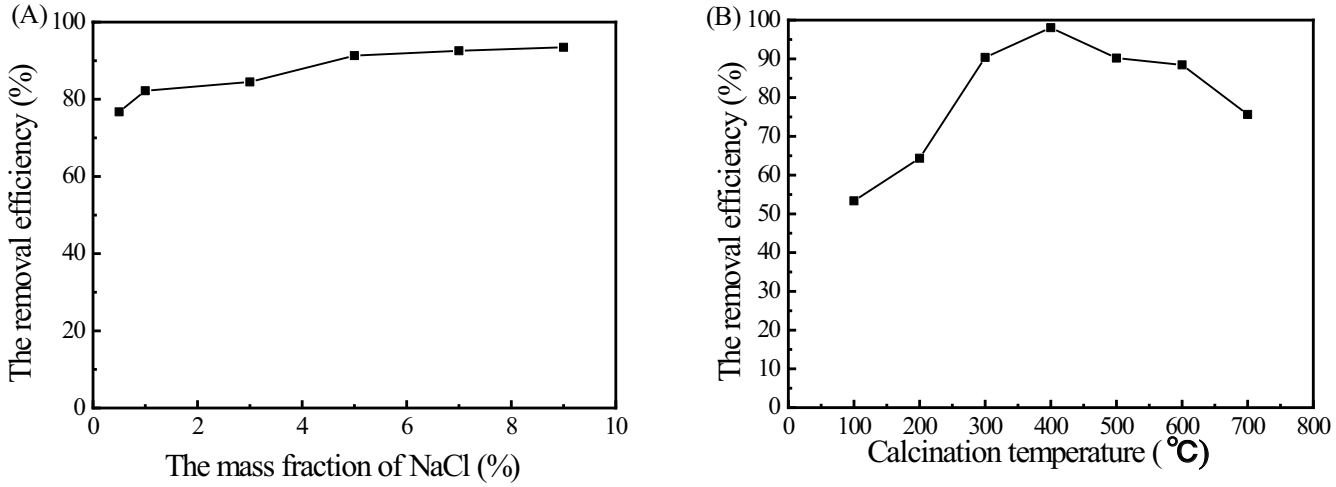

Fig. 1. (A) Effect of the mass fraction of modifier on the removal efficiency and (B) effect of the calcination temperature on the removal efficiency.

peak because sites on the surface of diatomite for Na attachment may be full when the mass fraction of NaCl was 5.00%.

The primary composition of diatomite is $SiO_2 \cdot nH_2O$, which contains a large part of free water and bound water. To further remove impurities and water in it, U-D-Na was calcinated at different temperatures, the result could be observed in Fig. 1B. The adsorption capacity of U-D-Na to phosphate reached a high point with the calcination temperature closed to 400°C. When the calcination was 400°C, it reached the best positive effect on removing organic impurities, water and other volatile substances; meanwhile, the structure of diatomite would not be damaged. If the calcination temperature exceeds 400°C, the structure of diatomite will be destroyed, resulting in poor phosphate removal efficiency. Hence U-D-Na should be prepared by calcination at 400°C.

3.1.2. Characterization of the adsorbent

The SEM graph of D, U-D, U-D-Na and the calcined U-D-Na is represented in Fig. 2. The appearance of D (Fig. 2A) was rough due to impurities attached to the surface. The U-D (Fig. 2B) had a uniform and clear aperture structure and enhanced permeability, which was beneficial for Na^+ dispersing to the surface and pores. The apart of holes of U-D-Na (Fig. 2C) were blocked since it resulted from Na introduction. The morphology of the calcined U-D-Na (Fig. 2D) showed the optimum surface structure that had best opened but not broken. The SEM images indicated that the modification method of U-D-Na has been applied successfully to diatomite.

The EDS of D, U-D, U-D-Na and the calcined U-D-Na is presented in Fig. 3. The main elements of diatomite were Si and O. Besides, diatomite contains a spot of Al, Fe, K, Ca and a trace of Ti and Mg. The content of various elements of diatomite changed little after ultrasonic and functionalization. Though the morphology feature of U-D was similar to U-D-Na, the presence of Na species in the adsorbent was verified by EDS of U-D-Na (Fig. 3C). The content of the attached Na was 00.82%, illustrating that Na successfully occupied the position on the surface of modified diatomite. Therefore, the adsorptive property of diatomite enhanced might be the existence of a certain amount of Na^+ which improved surface activity of diatomite.

The XRD pattern of D, U-D, U-D-Na and the calcined U-D-Na is shown in Fig. 4. The four kinds of samples had many similar spectral peaks in the X-ray diffraction pattern, and the spectral peaks were mainly at 20°–22° and 26°–27°, which proved that all samples have similar structures. The main spectrum peak at 26°~27° was demonstrated to be the characteristic spectrum peak of SiO_2, indicating that diatomite is composed of SiO_2 and contains a variety of impurities in small amounts. It is known that diatomite from Xundian belongs to clay-like diatomite that contains a variety of impurities. The spectral peak at 32° of the calcined U-D-Na was disappeared compared with other samples. The spectral peak at 32° may be the peak of organic impurity that decomposed and disappeared after calcination at 400°C. The XRD pattern indicated that the surface structure of diatomite had not been damaged by ultrasonic, functionalization and calcination.

The BET method was used to analyze the surface area, pore size, and pore volume. As can be seen in Fig. 5, diatomite is a mesoporous material that displays type II sorption behavior in the N_2 adsorption/desorption isotherms; the finding is consistent with the pore size distribution analysis in the inset. Table 3 summarizes the parameters of BET analysis, the surface area, pore size and pore volume of U-D were 22.48 m^2/g, 17.89 nm and 0.04855 cm^3/g, respectively. The BET parameters of U-D were larger than that of D, suggesting the microporous structure of diatomite was improved following ultrasonic. The surface area and pore volume of diatomite were decreased after Na-activation. The reason for this is easy to understand, and the drop in surface area and pore volume were caused due to the surface sites and pore being occupied by Na. After calcination in a muffle furnace at around 400°C, the surface area, pore size and pore volume of U-D-Na increased from 14.68 to 29.22 m^2/g, from 18.62 to 18.79 nm, from 0.03705 to 0.06301 cm^3/g, respectively. This result demonstrated that calcination further facilitated the surface area enlargement and pore development of diatomite. In a nutshell, the larger the surface area, pore size and pore volume would be suitable for adsorption, which was consistent with the discussion of SEM, EDS and XRD.

The functional groups of samples were characterized by FT-IR from Fig. 6. The absorption peaks of the four samples were similar and strong in many wavenumbers, and included absorption peaks of various oxygen-containing functional groups. Two absorption peaks at 539.99 and 476.35 cm^{-1} were attributed to the bending vibration of Si–O and Al–O, and two absorption peaks at 802.28 and 701.99 cm^{-1} were assigned to the stretching vibration of Si–O. The asymmetric stretching vibration absorption peak of CO_2 appeared in U-D-Na (Fig. 6C) at 2,352.83 cm^{-1}, and disappeared after calcination. The absorption peak of the

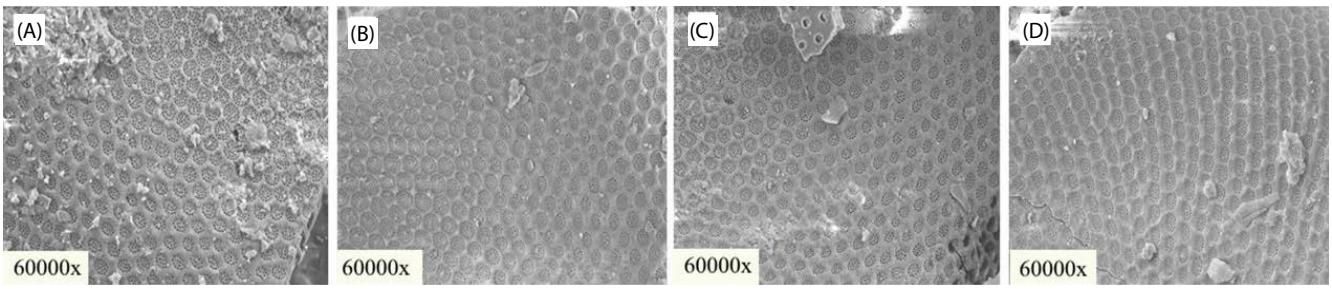

Fig. 2. Scanning electron micrographs for D (A), U-D (B), U-D-Na (C) and the calcined U-D-Na (D).

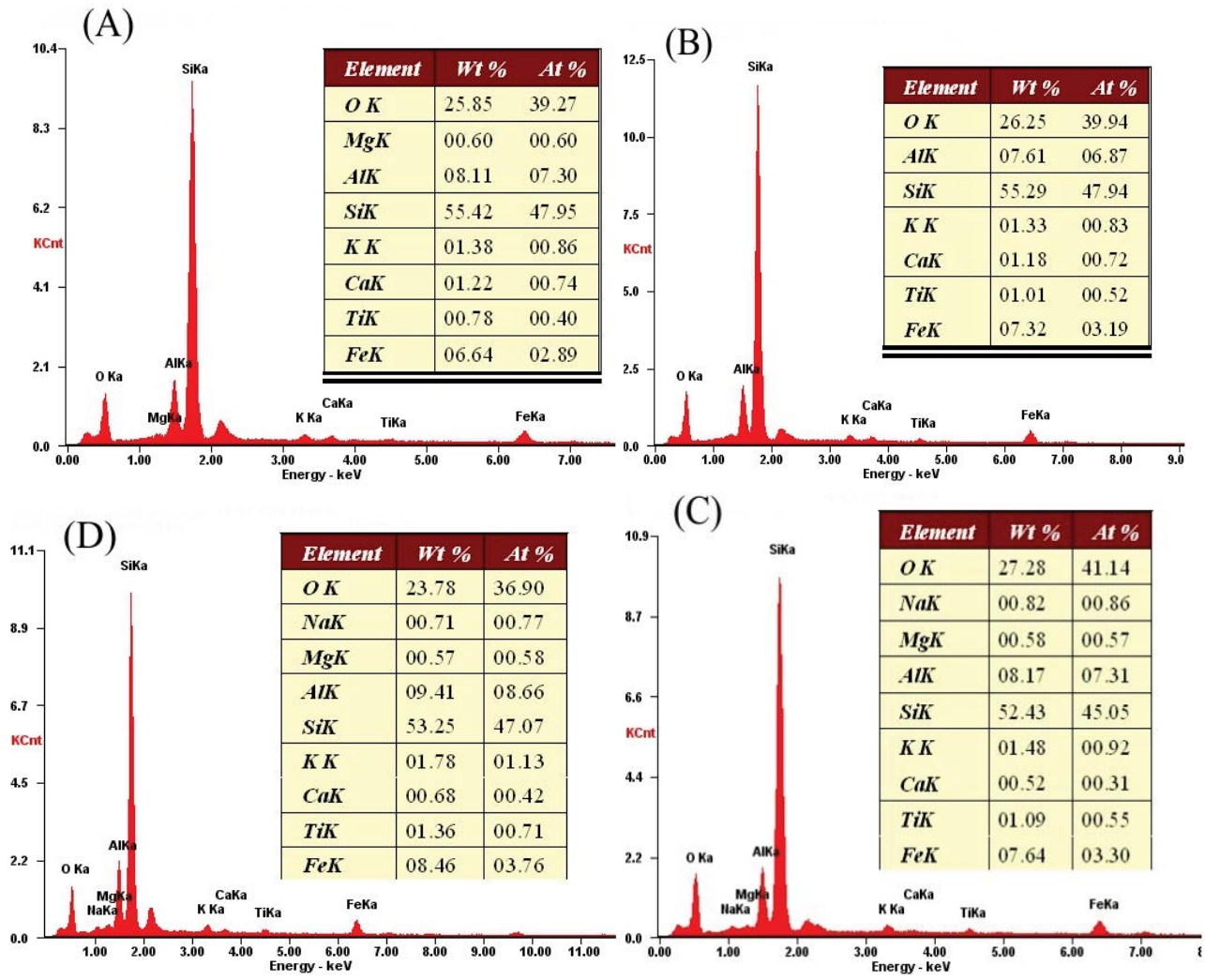

Fig. 3. Energy-dispersive X-ray spectroscopy for D (A), U-D (B), U-D-Na (C) and the calcined U-D-Na (D).

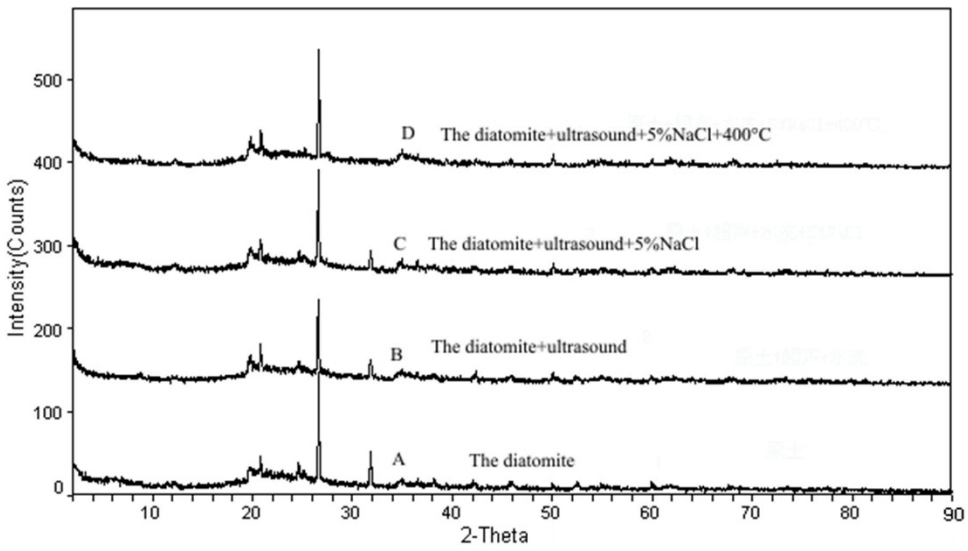

Fig. 4. XRD patterns of D (A), U-D (B), U-D-Na (C) and the calcined U-D-Na (D).

Table 3
BET surface area, pore size and pore volume for D, U-D, U-D-Na and the calcined U-D-Na

Parameter	D	U-D	U-Na-D	Calcined U-D-Na
Surface area (m^2/g)	20.87	22.48	14.68	29.22
Pore size (nm)	16.46	17.89	18.62	18.79
Pore volume (cm^3/g)	0.04548	0.04855	0.03705	0.06301

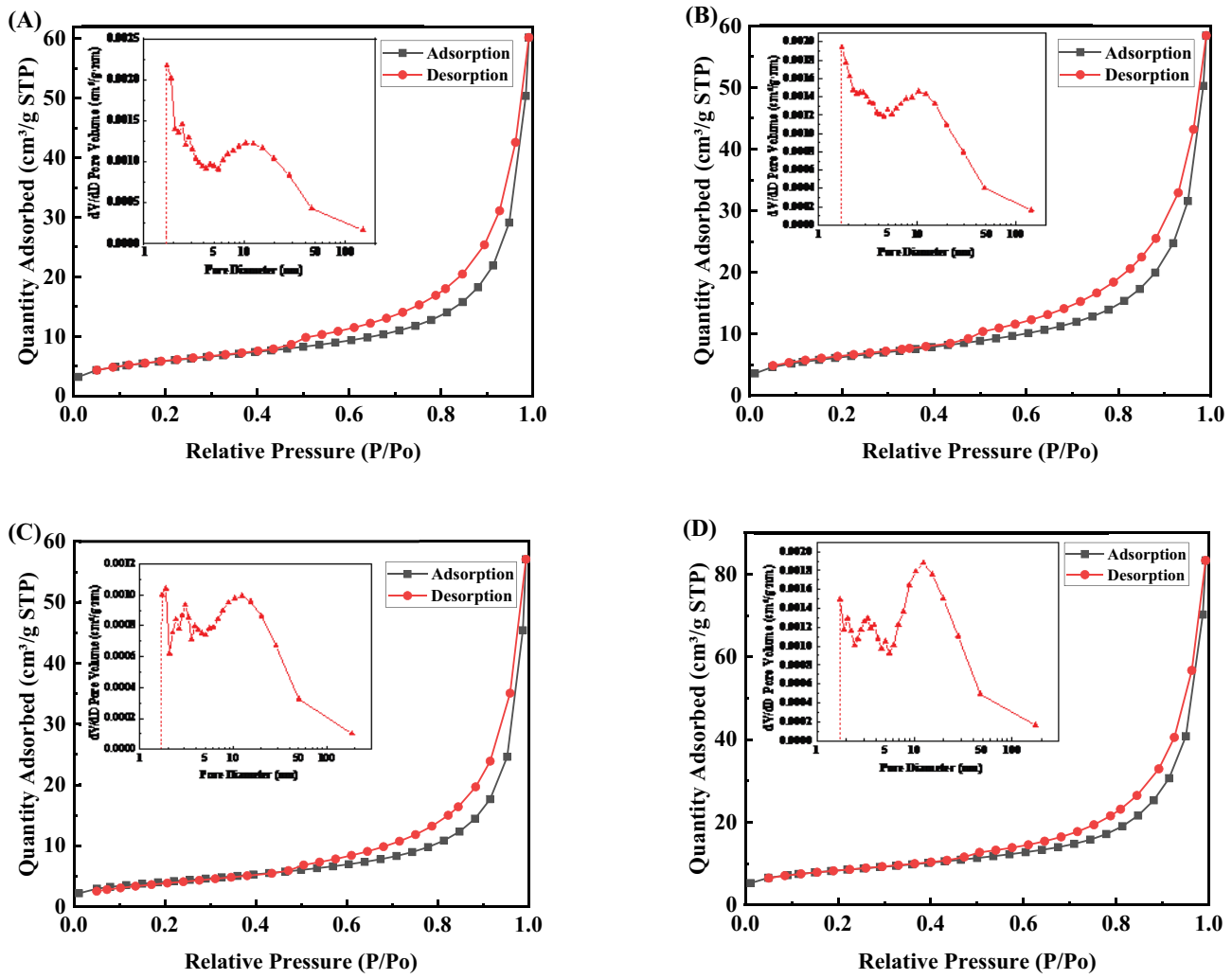

Fig. 5. N_2 adsorption/desorption isotherms of D (A), U-D (B), U-D-Na (C) and the calcined U-D-Na (D) (the inset: pore size distribution).

calcined U-D-Na (Fig. 6D) appeared at 1,639 cm^{-1}, which was corresponded to the bending vibration of O–H of bound water. The peaks at 3,629.53 and 3,704.53 cm^{-1} were assigned to the stretching vibration absorption peak of O–H. In the functionalization process, blocked pores were dredged stemming from the decomposition of organic impurities and free water, which had played a vital role in sustain the basic skeleton of diatomite. This fact was broadly stated in both FT-IR and TG/DSC curves and could be attributed to the method through ultrasonic, sodium modification and thermal treatment.

As it is depicted in Fig. 7, the dehydration temperatures, the weight loss rate and the thermal effects were confirmed by the DSC and TG curves. During the heating process, the TG curves of all samples showed two obvious weight loss peaks. In the first step, D showed weight loss of about 3.57% as the temperature reached up to 94.3°C, and the second weight loss was 18.90% as the temperature was above 334.0°C. The first weight loss temperature and weight loss rate of U-D were 90.5°C and 3.95% respectively, and the second weight loss rate reached 11.69% when the temperature was 360.2°C. The first weight loss rate

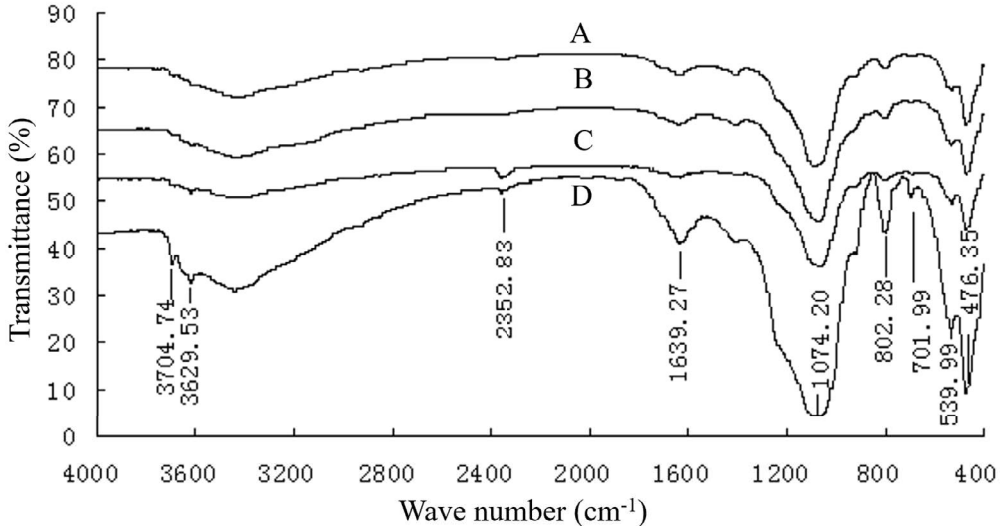

Fig. 6. The FT-IR spectral characteristics of D (A), U-D (B), U-D-Na (C) and the calcined U-D-Na (D).

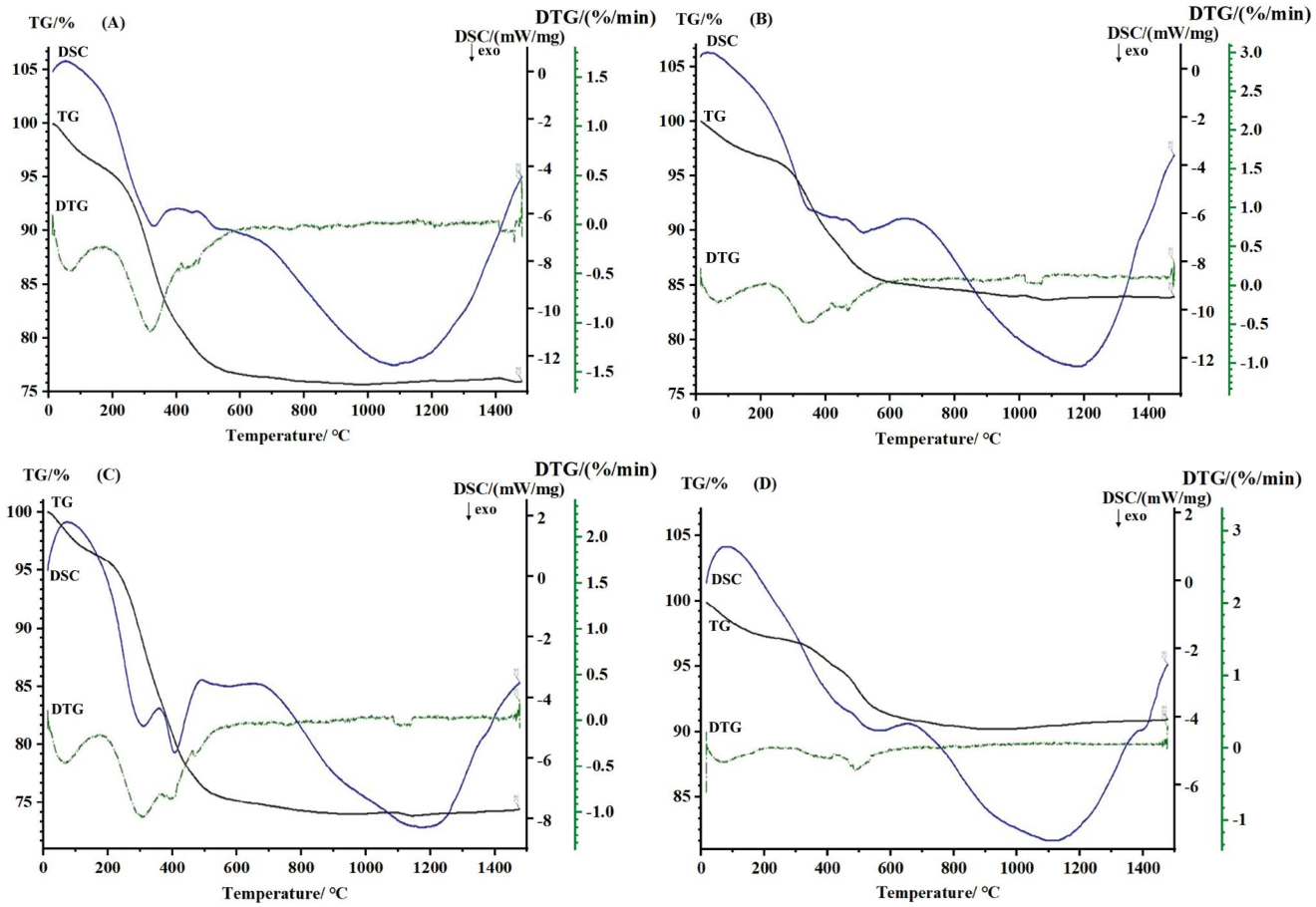

Fig. 7. STA of D (A), U-D (B), U-D-Na (C) and the calcined U-D-Na (D).

of U-D-Na was 3.95%, which occurred at approximately 92.6°C; the second weight loss rate of U-D-Na was 21.11% above 322.2°C. It is seen that the calcined U-D-Na first lost 2.67% at 87.8°C; the second weight loss rate was 6.02%, which occurred at approximately 491.8°C. In summary, the first weight loss temperature and weight loss rate of the calcined U-D-Na were lower than the other three samples. The possible reasons may be the effortless evaporation of water due to the decrease of surface impurities and the dredge of holes. Consequently, the thermostability of water located on the inner surface was decreased. By contrast, the second weight loss temperature of the calcined U-D-Na was significantly higher. It indicated that major impurities and water were eliminated in the calcination process.

3.2. Adsorption experiment

The contact time and temperature are key factors in the adsorption experiment, their effect is displayed in Fig. 8A. The removal efficiency of phosphate was increased rapidly in the beginning and then achieved equilibrium at 60 min. After the reaction reached the plateau line, the removal efficiency could be long-lasting. It was correlated with number of active functional groups of U-D-Na and restricted by the transmission rate of phosphate. The increasing tendency of the removal efficiency with the increase of temperature was not significant due to the stable performance of U-D-Na. The temperature would hardly influence the adsorption efficiency; thus U-D-Na was suitable for many water environments.

The dosage of adsorbent is one of the main factors that are regarded as a parameter impacting adsorption capacity. As can be seen from Fig. 8B, the removal efficiency of phosphate increased significantly when the dosage of U-D-Na ranges from 0.40 to 0.80 g. When the amount of adsorbent was increased above 0.80 g, the adsorption capacity had slightly risen. The active sites provided by the adsorbent were excessive when the amount of adsorbent was too much, but there was almost no phosphate left. The pH of the solution is a parameter that must be taken into consideration in the removal of phosphate. The adsorption process was carried out in the pH range 2–14, as is shown in Fig. 8C. The removal efficiency was relatively high at pH 6–12, and the results could be related to the existing forms of phosphorus at different pH values.

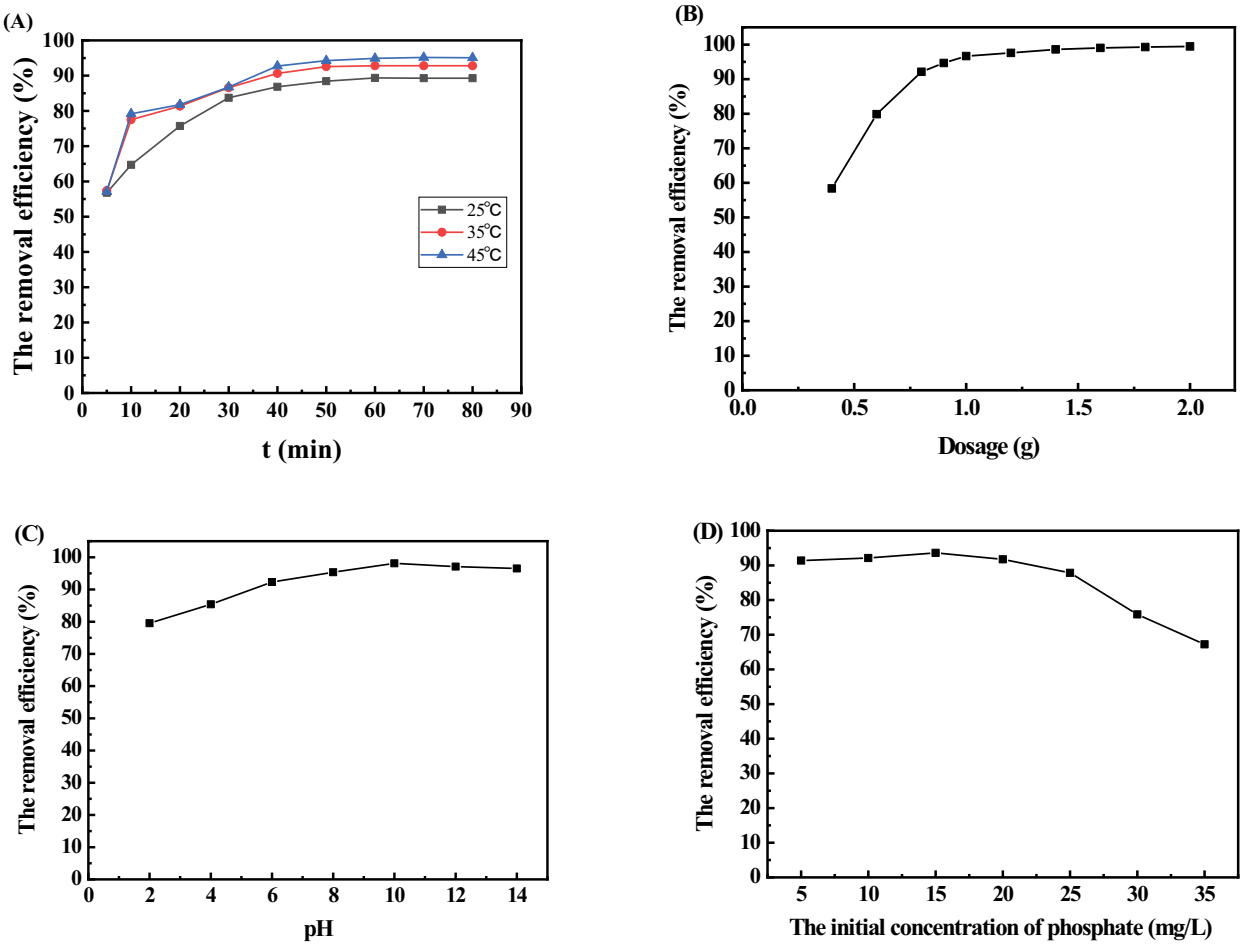

Fig. 8. Effects of contact time and temperature (A), dosage (B), pH (C) and initial concentration (D) on the removal efficiency of phosphate.

The initial concentration is a critical factor to be considered in the adsorption process. In Fig. 8D, the removal efficiency sharply dropped after the initial concentration of phosphate was greater than 25 mg/L. The removal efficiency declined at high concentration, because the number of active sites of each unit adsorbent was limited and the active sites only occupied by phosphate with a small amount. Therefore, the initial concentration of phosphate was determined at 25 mg/L.

3.3. Desorption and recycles experiments

The U-D-Na was regenerated five consecutive adsorption-d desorption cycles to evaluate its renewability. Several regenerant were used to desorb the phosphate adsorbed on the U-D-Na. The treatment effect of different regenerants is presented in Fig. 9 and Table 4. Among all the reagents, HCl had the best desorption and removal effect on the adsorbent. As depicted in Fig. 9A, when the mass fraction of HCl ranges from 1.00% to 7.00%, the desorption rate and removal efficiency tended rise considerably. The desorption rate and removal efficiency were dropped sharply when the mass fraction of the HCl reagent was greater than 7.00%; they reached a peak when the mass fraction of HCl was 7.00%. If the mass fraction of the HCl reagent is too high, the U-D-Na will absorb the ions of the HCl reagent to cover the surface and pores, which makes the phosphates difficult to be resolved from the adsorbent.

As shown in Fig. 9B, the adsorption efficiency kept a higher level off during the first four cycles, but the efficiency would be declined significantly after four consecutive recycles. Therefore, it is suggested that U-D-Na could be reutilized at least four times, and the operation cost was notably reduced.

3.4. Adsorption kinetic studies

Adsorption kinetics studies the adsorption rate and time when the equilibrium was reached. In this work, the adsorption data were fitted by the pseudo-first-order kinetic model, the pseudo-second-order kinetic model and the intra-particle diffusion model; the equations are as follows:

$$q_t = q_e\left(1 - e^{-k_1 t}\right) \tag{3}$$

$$q_t = \frac{k_2 q_e^2 t}{1 + k_2 q_e t} \tag{4}$$

$$q_t = k_p t^{1/2} + C \tag{5}$$

where q_e (mg/g) is the adsorption capacity at equilibrium; q_t (mg/g) is the adsorption amount of phosphate at time t; k_1 (min^{-1}) is a the pseudo-first-order kinetic rate constant and k_2 (g/(mg min)) is a pseudo-second-order kinetic rate constant; k_p (mg/(g $min^{1/2}$)) is the intra-particle diffusion rate constant.

The non-linear fitting curve results and the kinetic parameters are testified in Table 5 and Fig. S1A–D. The kinetic parameters calculated according to the pseudo-first-order kinetic model and the intra-particle diffusion model showed poor correlation. It proved that the pseudo-second-order kinetic model was fitted the adsorption process well (R > 0.9800), indicating that the chemisorption played a dominant role in the phosphate adsorption process.

Table 4
Effect of different reagent on the desorption rate and removal efficiency

Regenerant	Desorption rate (%)	Removal efficiency (%)
5.00% HCl	62.65	51.85
5.00% Na_2CO_3	48.25	46.80
5.00% NaOH	37.65	37.97
5.00% NaCl	19.47	15.67
Distilled water	5.84	3.04

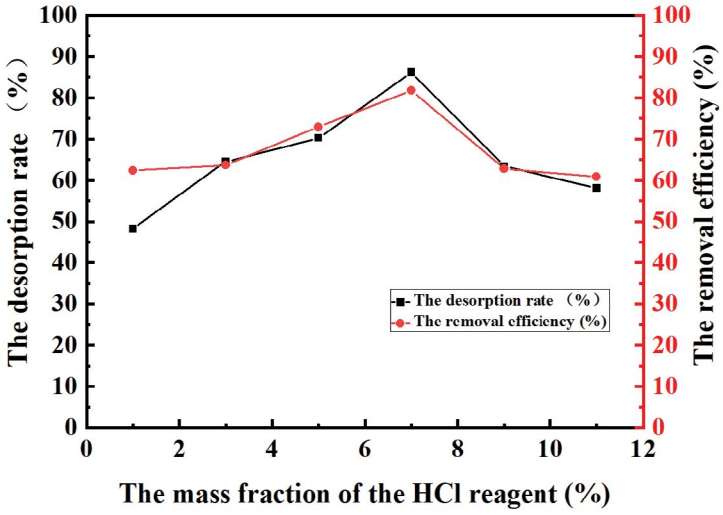

Fig. 9. Effect of the mass fraction of the HCl reagent on the desorption rate and removal efficiency.

Table 5
The pseudo-first-order, the pseudo-second-order kinetic and the intraparticle diffusion model parameters

T/K	Pseudo-first-order kinetic			Pseudo-second-order kinetic			Intraparticle diffusion model		
	k_1	q_e	R	k_2	q_e	R	k_p	C	R
298	0.1677	1.353	0.9072	0.1796	1.467	0.9821	0.3560	0.4037	0.9644
308	0.1922	1.413	0.9540	0.2048	1.519	0.9871	0.3304	0.5350	0.9241
318	0.1863	1.441	0.9412	0.1881	1.556	0.9803	0.3538	0.5011	0.9273

3.5. Adsorption isotherm

The adsorption isotherm correlates the equilibrium concentration of phosphate with the equilibrium adsorption capacity in the solution at different temperatures, indicating the distribution of adsorbed molecules between liquid and solid phases. Langmuir, Freundlich and Temkin adsorption isotherms were used in the present study. The adsorption isotherm model was calculated from the following equations:

$$q_e = \frac{q_m k_L C_e}{1 + k_L C_e} \tag{6}$$

$$q_e = k_F C_e^{1/n} \tag{7}$$

$$q_e = \frac{RT}{b}\ln C_e + \frac{RT\ln k_T}{b} = A + B\ln C_e \tag{8}$$

where q_e (mg/g) is the adsorption capacity at equilibrium, q_m (mg/g) is the saturated adsorption capacity, and C_e (mg/L) is the equilibrium concentration of phosphorus; k_L (L/mg) is the equilibrium constant that related to temperature and heat of adsorption; k_F ((mg/g)(L/mg)$^{1/n}$) and n are calculated from the Freundlich equation, which indicates adsorption capacity and adsorption intensity, respectively; k_T (L/g) is the equilibrium binding constant, and b is Temkin constant.

The non-linear fitting curves and data of Freundlich, Langmuir and Temkin have given in Table 6 and Fig. S2A–D. The nonlinear coefficient (R = 0.9948) of the Langmuir isothermal fitting equation showed a well correlation; the adsorption process of phosphate follows the Langmuir adsorption model better than Freundlich and Temkin adsorption isotherms. According to the Langmuir adsorption isotherm theory, the adsorption process was a monolayer surface adsorption [29], indicating that phosphate was bound to the surface of U-D-Na in the form of a single molecular layer. The theoretical maximum phosphate adsorption capacity of U-D-Na calculated by the Langmuir model was 1.459 mg/g.

3.6. Thermodynamic studies

The physicochemical properties of the adsorption processes can be illustrated by the Gibbs free energy ($\Delta G°$), enthalpy change ($\Delta H°$), and entropy change ($\Delta S°$). The thermodynamic parameters were determined by:

$$\Delta G° = -RT\ln k_c \tag{9}$$

$$\ln k_c = \frac{\Delta S°}{R} - \frac{\Delta H°}{\mathrm{RT}} \tag{10}$$

where R (8.314 J/mol/K) is gas constant, T (K) is a temperature in Kelvin and k_c (L/g) is the thermodynamic equilibrium constant.

The enthalpy change ($\Delta H°$) and entropy change ($\Delta S°$) were calculated by the chart of lnk_c vs. 1/T, the results are listed in Table 7. The $\Delta H°$ value was positive, indicating that the adsorption process of phosphate was endothermic in nature. The $\Delta S°$ value had a positive sign, reflecting that the disorder degree of the solid-liquid interface increased during the adsorption process. The negative value of $\Delta G°$ testified that the adsorption process has the nature of spontaneous and feasibility [30,31].

3.7. Possible adsorption mechanism

The adsorption mechanism is closely related to the structure of sorbent and the existing-form of phosphate. The surface of diatomite exists the hydrolysis fracture reaction of Si–O bond, and the R-OH is generated after the hydrolysis fracture reaction. R-OH can further react with H^+ and OH^- due to its amphoteric nature. The zero charge point of diatomite is about 2, hence the surface of diatomite has a positive charge when the pH value of the solution is less than 2 [16]. The negatively charged surface is not conducive to the adsorption of phosphate owing to the electrostatic repulsion. Therefore, the method that added Na^+ to diatomite can improve the overall zero charge point of diatomite and make it acquire a positive charge in the solution with a wide pH range [16], which is conducive to the adsorption of phosphate.

Table 6
Freundlich, Langmuir and Temkin isotherm parameters

Freundlich			Langmuir			Temkin		
k_F	n	R	k_L	q_m	R	A	B	R
0.7920	3.381	0.8743	1.351	1.459	0.9948	0.7740	0.3535	0.9283

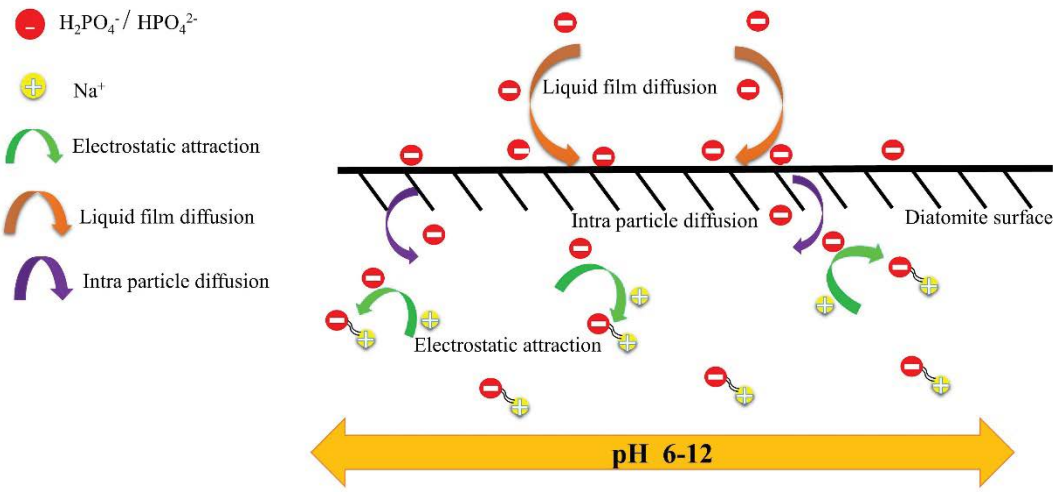

Fig. 10. Schematic diagram for the mechanism of U-D-Na removed phosphate.

Table 7
Thermodynamic parameters for the adsorption of phosphate onto U-Na-D

$\Delta H°$ (kJ/mol)	$\Delta S°$ (kJ/mol/K)	$\Delta G°$ (kJ/mol)		
		298 K	308 K	318 K
33.24	0.1061	–31.60	–32.65	–33.72

In the aqueous solution, phosphate existed in the form of H_3PO_4, $H_2PO_4^-$, HPO_4^{2-}, and PO_4^{3-} in different pH [32]. When pH ranging from 5 to 7, the phosphate in water is basically $H_2PO_4^-$. HPO_4^{2-} is primarily found in aqueous solutions when pH is between 7 and 10. HPO_4^{2-} and PO_4^{3-} mainly exist in aqueous solutions at pH 10–12. In electrostatic adsorption, the phosphate form with a more negative charge might have a greater adverse effect [33]. At pH 6–12 the adsorption efficiency of U-D-Na was the highest, and the most phosphate was absorbed positive charge on the surface of U-D-Na by electrostatic attraction due to abundant $H_2PO_4^-$ and HPO_4^{2-}. Besides, the adsorption process conforms to the pseudo-second-order kinetic model and Langmuir isotherm, which indicates that the adsorption process is mainly a chemical process; and it is spontaneous and endothermic monolayer chemisorption. The possible reaction occurs as shown in Eqs. (11)–(15) [16,26]:

$$R \equiv OH + H^+ \rightarrow R \equiv OH_2 \quad (11)$$

$$R \equiv OH + OH^- \rightarrow R \equiv O^- + H_2O \quad (12)$$

$$R \equiv O^- + Na^+ \rightarrow R \equiv O - Na \quad (13)$$

$$Na^+ + H_2PO_4^- \rightarrow NaH_2PO_4 \quad (14)$$

$$Na^+ + HPO_4^{2-} \rightarrow Na_2H_2PO_4 \quad (15)$$

As seen in Fig. 10, the following processes may occur during adsorption: (1) the liquid film diffusion, large amounts of phosphate migrate from the solution to the surface of the adsorbent; (2) the intraparticle diffusion, phosphate diffuses into the pores of adsorbent; (3) phosphate is adsorbed at the active group inside the adsorbent.

4. Conclusion

An efficient adsorbent was prepared from the diatomite via ultrasonic and NaCl solution to reduce the content of phosphorus in the water. The U-D-Na has advantages of facile preparation technology, excellent regeneration capacity and low-cost; it realizes efficient phosphate adsorption in the water. The removal efficiency of phosphate was close to 90% and above when the dosage of adsorbent is 0.80 g, contact time is 60 min, temperature is room temperature, pH is 6–12 and the initial concentration of phosphate is 25 mg/L. Base on the pseudo-second-order kinetic model, the Langmuir isotherm model and thermodynamic parameters, a possible explanation is that the adsorption process is a spontaneous and heat-absorbing monolayer adsorption in which chemical adsorption plays a major role, and the adsorption of phosphate through electrostatic attraction. This possible adsorption mechanism sets a foundation for the wide application of U-D-Na in water environment protection.

Acknowledgements

This work was supported by the Science Research Fund Projects of Department of Education of Yunnan Province (No. 2020J0327), the Science Research Fund Projects of Department of Education of Yunnan Province (No.2020J0329) and the 2020 Undergraduate Innovation and Entrepreneurship Training Projects of Yunnan Minzu University (No.2020DC64).

References

[1] D.W. Schindler, S.R. Carpenter, S.C. Chapra, R.E. Hecky, D.M. Orihel, Reducing phosphorus to Curb Lake eutrophication is a success, Environ. Sci. Technol., 50 (2016) 8923–8929.

[2] S.K. Ramasahayam, L. Guzman, G. Gunawan, T. Viswanathan, A comprehensive review of phosphorus removal technologies and processes, J. Macromol. Sci. Part A Pure Appl. Chem., 51 (2014) 538–545.
[3] Q. Yin, B. Zhang, R. Wang, Z. Zhao, Biochar as an adsorbent for inorganic nitrogen and phosphorus removal from water: a review, Environ. Sci. Pollut. Res., 24 (2017) 26297–26309.
[4] Z. Sun, X. Yang, G. Zhang, S. Zheng, R.L. Frost, A novel method for purification of low grade diatomite powders in centrifugal fields, Int. J. Miner. Process., 125 (2013) 18–26.
[5] J.L. Barnard, P. Dunlap, M. Steichen, Rethinking the mechanisms of biological phosphorus removal, Water Environ. Res., 89 (2017) 2043–2054.
[6] G. Ru, Research progresses of phosphorus removal technologies of eutrophic water, Guangdong Chem. Ind., 44 (2017) 100–114.
[7] Z. Ajmal, A. Muhmood, M. Usman, S. Kizito, J.X. Lu, R.J. Dong, S.B. Wu, Phosphate removal from aqueous solution using iron oxides: adsorption, desorption and regeneration characteristics, J. Colloid Interface Sci., 528 (2018) 145–155.
[8] D. Mitrogiannis, M. Psychoyou, I. Baziotis, J.I. Vassilis, N. Koukouzas, N. Tsoukalas, D. Palles, E. Kamitsos, G. Oikonomou, G. Markou, Removal of phosphate from aqueous solutions by adsorption onto $Ca(OH)_2$ treated natural clinoptilolite, Chem. Eng. J., 320 (2017) 510–522.
[9] S.D. Gisi, G. Lofrano, M. Grassi, M. Notarnicola, Characteristics and adsorption capacities of low-cost sorbents for wastewater treatment: a review, Sustainable Mater.Technol., 9 (2016) 10–40.
[10] G.R. Dong, Z.Q. Su, J.B. Wang, Diatomite modification and its application in wastewater treatment, Adv. Mater. Res., 850–851 (2013) 1355–1359.
[11] C. Jiang, L. Jia, Y. He, B. Zhang, G. Kirumba, J. Xie, Adsorptive removal of phosphorus from aqueous solution using sponge iron and zeolite, J. Colloid Interface Sci., 402 (2013) 246–252.
[12] D. Mahardika, H.S. Park, K.H. Choo, Ferrihydrite-impregnated granular activated carbon (FH@GAC) for efficient phosphorus removal from wastewater secondary effluent, Chemosphere, 207 (2018) 527–533.
[13] X. Chen, L. Wu, F. Liu, P. Luo, X. Zhuang, J. Wu, Z. Zhu, S. Xu, G. Xie, Performance and mechanisms of thermally treated bentonite for enhanced phosphate removal from wastewater, Environ. Sci. Pollut. Res. Int., 25 (2018) 15980–15989.
[14] G. Zhang, D. Cai, M. Wang, C. Zhang, J. Zhang, Z. Wu, Microstructural modification of diatomite by acid treatment, high-speed shear, and ultrasound, Microporous Mesoporous Mater., 165 (2013) 106–112.
[15] L. Xie, P. Wang, Z. Li, W. Xie, Y. Wu, M. Kuang, X. Li, Preparation of Zn_2SiO_4/diatomite composites and its performance of adsorption methylene blue, Bull. Chinese Ceram. Soc., 39 (2020) 974–979.
[16] W. Cui, H. Ai, S. Zhang, J. Wei, Research status on application of modified adsorbents in phosphorus removal from wastewater, Chem. Ind. Eng. Prog., 39 (2020) 4210–4226.
[17] P. Xia, X. Wang, X. Wang, J. Zhang, H. Wang, J. Song, R. Ma, J. Wang, J. Zhao, Synthesis and characterization of MgO modified diatomite for phosphorus recovery in eutrophic water, J. Chem. Eng. Data, 62 (2016) 226–235.
[18] Y. Wang, X. Zhang, Y. Wei, X. Zhong, Research on the adsorption capability of diatomite-loaded lanthanum for phosphate radicals in water, Ind. Water Treat., 39 (2019) 41–44.
[19] G. Lyngsie, K. Katika, I.L. Fabricius, H.C.B. Hansen, O.K. Borggaard, Phosphate removal by iron oxide-coated diatomite: laboratory test of a new method for cleaning drainage water, Chemosphere, 222 (2019) 884–890.
[20] Y. Fan, Z. Wang, L. Zhao, D. Wu, Modification of diatomite by zirconium and its performance in phosphate removal from water, Environ. Sci., 38 (2017) 1490–1496.
[21] F. Zhang, M. Cheng, Z. Sun, L. Wang, Q. Zhou, X. Huang, Combined acid rain and lanthanum pollution and its potential ecological risk for nitrogen assimilation in soybean seedling roots, Environ. Pollut., 231 (2017) 524–532.
[22] W. Sun, G. Ma, Y. Sun, Y. Liu, N. Song, Y. Xu, H. Zheng, Effective treatment of high phosphorus pharmaceutical wastewater by chemical precipitation, Can. J. Chem. Eng., 95 (2017) 1585–1593.
[23] Z. Zhang, X. Liu, D. Li, Y. Lei, T. Gao, B. Wu, J. Zhao, Y. Wang, G. Zhou, H. Yao, Mechanism of ultrasonic impregnation on porosity of activated carbons in non-cavitation and cavitation regimes, Ultrason. Sonochem., 51 (2019) 206–213.
[24] C. Jin, Y. Du, Y. Li, X. Wang, Y. Niu, H. Gu, S. Li, Synthesise of amino-functionalized diatomite and adsorption of Pb(II) and Cr(VI), China Powder Sci. Technol., 26 (2020) 1–8.
[25] Q.Y. Dong, Y.C. Fang, B. Tan, A. Ontiveros-Valencia, A. Li, H.P. Zhao, Antimonate removal by diatomite modified with Fe-Mn oxides: application and mechanism study, Environ. Sci. Pollut. Res., 28 (2021) 13873–13885.
[26] Y. Wu, X. Li, Q. Yang, D. Wang, Q. Xu, F. Yao, F. Chen, Z. Tao, X. Huang, Hydrated lanthanum oxide-modified diatomite as highly efficient adsorbent for low-concentration phosphate removal from secondary effluents, J. Environ. Manage., 231 (2019) 370–379.
[27] J. Li, X. Fang, M. Yang, W. Tan, H. Zhang, Y. Zhang, G. Li, H. Wang, Simultaneous recovery of microalgae, ammonium and phosphate from simulated wastewater by MgO modified diatomite, Chem. Eng. J., 362 (2019) 802–811.
[28] Y. Pei, M. Wang, D. Tian, X. Xu, L. Yuan, Synthesis of core-shell SiO_2@MgO with flower like morphology for removal of crystal violet in water, J. Colloid Interface Sci., 453 (2015) 194–201.
[29] Patiha, E. Heraldy, Y. Hidayat, M. Firdaus, The Langmuir isotherm adsorption equation: the monolayer approach, IOP Conf. Ser.: Mater. Sci. Eng., 107 (2016) 012067.
[30] I. Anastopoulos, G.Z. Kyzas, Are the thermodynamic parameters correctly estimated in liquid-phase adsorption phenomena, J. Mol. Liq., 218 (2016) 174–185.
[31] E.C. Lima, A.A. Gomes, H.N. Tran, Comparison of the nonlinear and linear forms of the van't Hoff equation for calculation of adsorption thermodynamic parameters ($\Delta S°$ and $\Delta H°$), J. Mol. Liq., 311 (2020) 113315, doi: 10.1016/j.molliq.2020.113315.
[32] Y.F. Lin, H.W. Chen, Y.C. Chen, C.S. Chiou, Application of magnetite modified with polyacrylamide to adsorb phosphate in aqueous solution, J. Taiwan Inst. Chem. Eng., 44 (2013) 45–51.
[33] J. Li, X. Fang, M. Yang, W. Tan, H. Zhang, Y. Zhang, G. Li, H. Wang, The adsorption properties of functionalization vetiver grass-based activated carbon: the simultaneous adsorption of phosphate and nitrate, Environ. Sci. Pollut. Res., 28 (2020) 40544–40554.

Supporting information

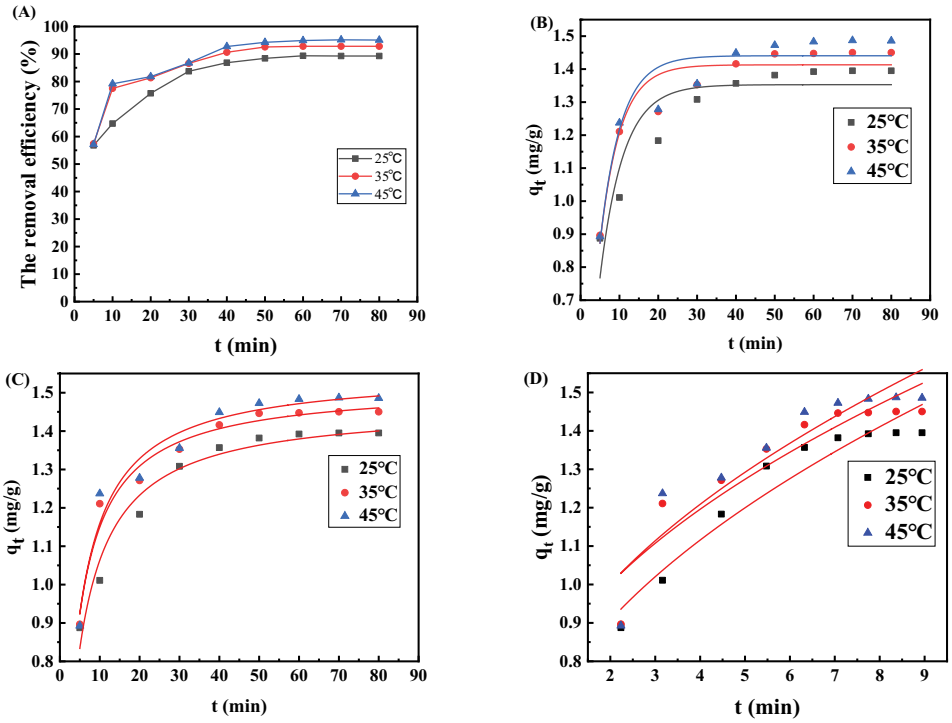

Fig. S1. (A) Kinetic adsorption curves at different temperatures. (B) Non-linear curve fitting of kinetic data to pseudo-first-order model. (C) Non-linear curve fitting of kinetic data to pseudo-second-order model. (D) Non-linear curve fitting of kinetic data to intra-particle diffusion model.

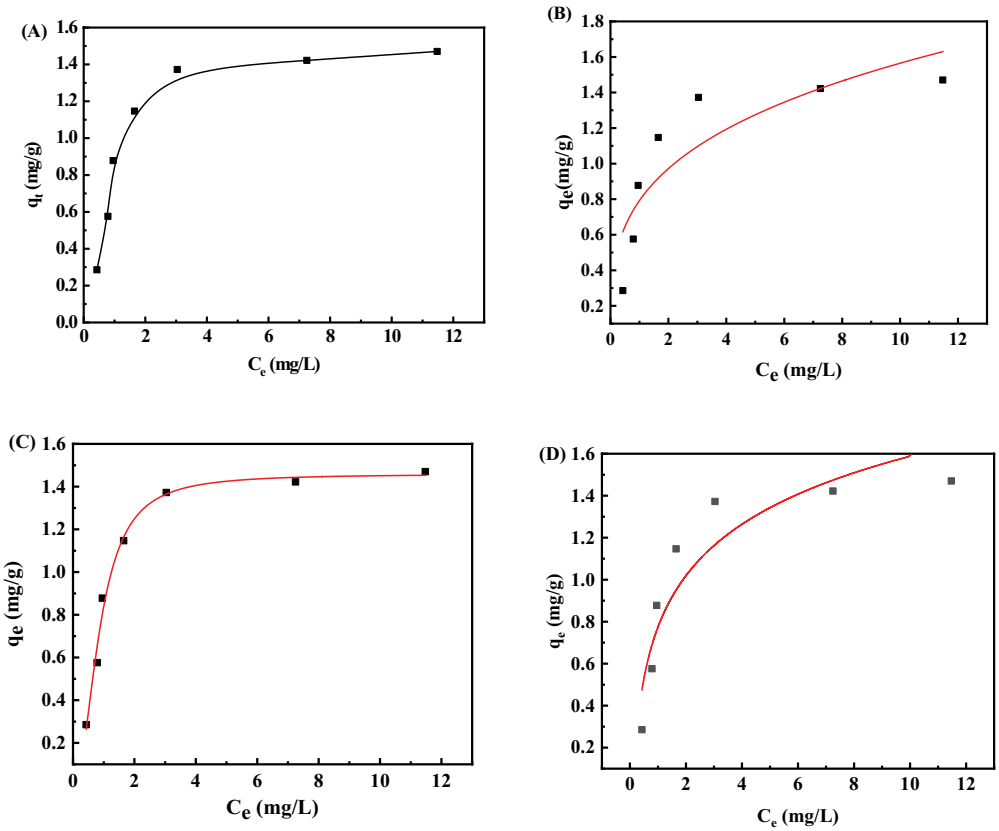

Fig. S2. (A) Isotherms of phosphate on U-D-Na. (B) Non-linear fitting curve of Freundlich adsorption isotherms. (C) Non-linear fitting curve of Langmuir adsorption isotherms. (D) Non-linear fitting curve of Temkin adsorption isotherms.